Magnetic Field and Gravitational Waves from the First-Order Phase Transition

Yuefeng Di, Jialong Wang, Ruiyu Zhou, and Ligong Bian*
Department of Physics, Chongqing University, Chongqing 401331, China

Rong-Gen Cai†
CAS Key Laboratory of Theoretical Physics, Institute of Theoretical Physics, Chinese Academy of Sciences, P.O. Box 2735, Beijing 100190, China,
School of Physical Sciences, University of Chinese Academy of Sciences, No. 19A Yuquan Road, Beijing 100049, China,
and School of Fundamental Physics and Mathematical Sciences, Hangzhou Institute for Advanced Study, University of Chinese Academy of Sciences, Hangzhou 310024, China

Jing Liu‡
School of Fundamental Physics and Mathematical Sciences, Hangzhou Institute for Advanced Study, University of Chinese Academy of Sciences, Hangzhou 310024, China
and School of Physical Sciences, University of Chinese Academy of Sciences, Beijing 100049, China

(Received 6 February 2021; accepted 27 May 2021; published 24 June 2021)

We perform the three-dimensional lattice simulation of the magnetic field and gravitational wave productions from bubble collisions during the first-order electroweak phase transition. Except for the gravitational wave, the power-law spectrum of the magnetic field strength is numerically calculated for the first time, which is of a broken power-law spectrum: $B_\xi \propto f^{0.91}$ for the low-frequency region of $f < f_\star$ and $B_\xi \propto f^{-1.65}$ for the high-frequency region of $f > f_\star$ in the thin-wall limit, with the peak frequency being $f_\star \sim 5$ Hz at the phase transition temperature 100 GeV. When the hydrodynamics is taken into account, the generated magnetic field strength can reach $B_\xi \sim 10^{-7}$ G at a correlation length $\xi \sim 10^{-7}$ pc, which may seed the large scale magnetic fields. Our study shows that the measurements of cosmic magnetic field strength and gravitational waves are complementary to probe new physics admitting electroweak phase transition.

DOI: 10.1103/PhysRevLett.126.251102

Introduction.—Recent lattice simulation confirms that there is no first-order phase transition (PT) in the Standard Model (SM) [1]. However, a first-order electroweak PT is a general feature in many new physics models beyond the SM, which provides one crucial Sakharov condition for the explanation of the baryon asymmetry of the Universe in the paradigm of electroweak baryogenesis [2]. New physics models admitting a first-order PT can be explored at future high-energy colliders through the probe of the Higgs pair production [3]. The study of first-order PT has seen growing interest of particle physicists after the LIGO and Virgo Collaborations released their direct detection of gravitational waves (GWs) [4], since a general prediction of the first-order PT, i.e., the stochastic gravitational waves backgrounds, open a new astronomy window to probe new physics beyond the SM [5–7]. The GWs from the first-order electroweak PT is an important scientific goal of Laser Interferometer Space Antenna (*LISA*) [8], Taiji [9], TianQin [10], Big Bang Observer (BBO) [11], and Decihertz Interferometer Gravitational Wave Observatory (DECIGO) [12]. On the other hand, the ubiquitous existence of the cosmological magnetic fields (MFs) is confirmed by observations [13–16], especially the lower bounds on intergalactic MFs were derived from gamma-ray observations of blazars [17–19]. However, the origin of the large scale MFs is still a mystery. The first-order PT is proposed to produce the MFs [20–25], which may seed the cosmic MFs. Vachaspati [20] proposed to generate the MFs with the nonvanishing gradients of the Higgs fields when the bubbles collide during the first-order electroweak PT.

In this Letter, we intend to numerically study the production of MFs and GWs during the PT process where bubble collision occurs and investigate the possibility to probe the first-order electroweak PT directly with observations of MFs and GWs. We numerically calculate the MF spectrum and GW energy spectrum, where the effects of the bubble wall thickness and the Higgs gradients' contribution to the MFs generation are explored. The previous study of MFs generation in Ref. [26] did not consider the GW production. We study the generations of the MFs and GWs together for the first time. We perform a three-dimensional lattice simulation of Higgs and electroweak gauge fields rather than solely adopting a scalar theory as the previous GWs simulations [27]. [References [28,29] studied the

bubble collision in the U(1) gauge theory.] Our simulations consider the first-order PT, admitting GWs production from bubble collisions rather than preheating in the hybrid inflation [30,31]. Since the duration time of the first-order PT is much smaller than the Hubble time, we neglect the effect of expansion of the Universe throughout this Letter.

The PT model.—To study the generation of MFs, we first present the relevant Lagrangian in the electroweak theory,

$$\mathcal{L} = |D_\mu \Phi|^2 - \frac{1}{4} W^a_{\mu\nu} W^{a\mu\nu} - \frac{1}{4} B_{\mu\nu} B^{\mu\nu} - V(\Phi). \quad (1)$$

Here Φ and $V(\Phi)$ denote Higgs field and the Higgs potential, the covariant derivative is $D_\mu = \partial_\mu - i(g/2)\sigma^a W^a_\mu - i(g'/2)B_\mu$, where σ^a $(a = 1, 2, 3)$ are the Pauli matrices, and the $\mathrm{SU}(2)_L$ and $\mathrm{U}(1)_Y$ field strengths are $W^a_{\mu\nu}$ and $B_{\mu\nu}$, respectively. The physical values of the coupling constants are $g = 0.65$ and $g' = 0.53g$. A first-order PT can be realized in many models beyond the SM, such as SM extended with a dimensional-six operator $(\Phi^\dagger\Phi)^3/\Lambda^2$ [32–34], real singlet-extended standard model [35–41], two-Higgs-doublet model [42–47], the George-Macheck model [48], and next-to minimal supersymmetric standard model [49,50]. In these models, the Higgs potential $V(\phi)$ embracing a barrier at finite temperature that can trigger a first-order PT proceeding with bubble nucleations and collisions [32] that are expected to produce MFs [21,23,24] and GWs [33]. The correspondence between model parameters of the $V(\phi)$ at the PT temperature and bubble characteristics (mean bubble separation, wall thickness, and wall velocity) can be obtained as in Refs. [51–54]. The initial conditions are set as $\Phi = \dot{\Phi} = 0$, and the profile of generated bubbles is adopted as

$$\Phi(t = 0, \boldsymbol{r}) = \frac{v}{2}\left[1 - \tanh\left(\frac{r - R_0}{L_w}\right)\right]\begin{pmatrix} 0 \\ 1 \end{pmatrix}, \quad (2)$$

where R_0 is the initial bubble radius and L_w is the thickness of the critical bubble wall, which is highly related with the potential barrier when the phase transition occurs. Following Ref. [27], we define the "wall" of the bubble corresponding to the section of the field profile between $r_{\mathrm{in}}(t)$ and $r_{\mathrm{out}}(t)$, where $\phi(t, r_{\mathrm{in}}) = v[1 - \tanh(-1/2)]/2$ and $\phi(t, r_{\mathrm{out}}) = v[1 - \tanh(1/2)]/2$. Here v is the Higgs expectation value of the true vacuum. We consider that the bubbles randomly nucleate in the regions where the symmetry is unbroken to capture the dynamic of the first-order PT, where the bubble nucleation rate is directly connected with the mean bubble separation (see Supplemental Material [55], which includes [27,51,56,57]). We use the temporal gauge, $W^a_0 = B_0 = 0$, and evolve the equations of motion (EOM) for bosonic fields on the lattice as Refs. [58,59] (see Supplemental Material [55]) to generate the MFs and GWs. We note that, in the previous simulations of GWs from first-order PT, the electroweak gauge fields are absent in the EOM of bosonic fields; our simulation shows that its effect is indeed negligible for GW production, due to the smallness of the MF energy, as can be found in Fig. 1. Meanwhile, the evolution of gauge fields here seeds the MFs production during the first-order PT.

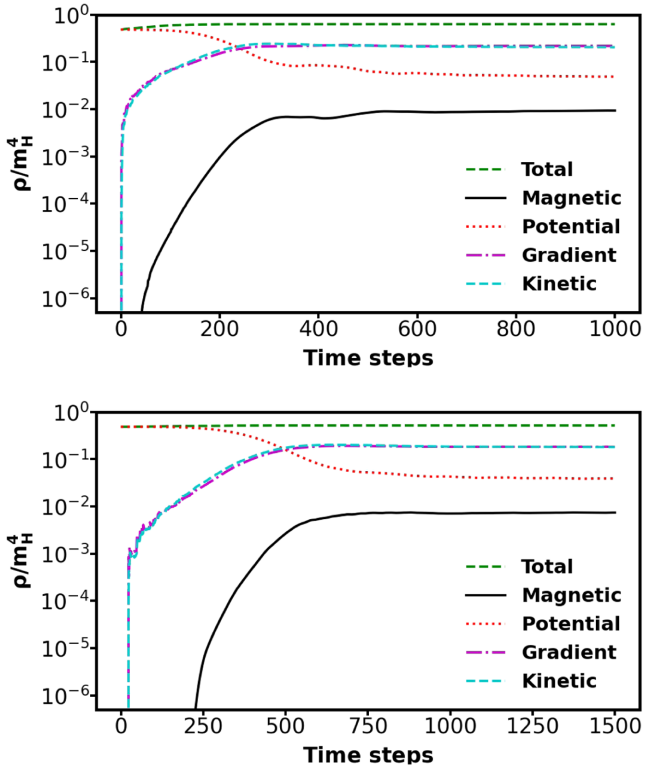

FIG. 1. The energy density evolution of different ingredients for bubble nucleation rates $p_B = 10^{-8}$ (top) and $p_B = 10^{-9}$ (bottom).

MF and GW production.—We define the electromagnetic fields after the Higgs field leaves the symmetric phase as $A_\mu = \sin\theta_w n^a W^a_\mu + \cos\theta_w B_\mu$, where θ_w is the weak mixing angle satisfying $\sin^2\theta_w = 0.22$, and $n^a \equiv -(\Phi^\dagger\sigma^a\Phi)/v^2$ presents the direction of the Higgs field. The corresponding field strength is constructed as [60,61]

$$A_{\mu\nu} = \sin\theta_w n^a W^a_{\mu\nu} + \cos\theta_w B_{\mu\nu} - i\frac{2}{gv^2}\sin\theta_w \times [(D_\mu\Phi)^\dagger(D_\nu\Phi) - (D_\nu\Phi)^\dagger(D_\mu\Phi)]. \quad (3)$$

One can see that the field strength tensor [Eq. (3)] for the calculation of MF strength includes the contributions from the Higgs gradients, whose effects depend on the bubble collision dynamics that will be investigated later. Following the conventions in Refs. [62,63], MFs can be described in terms of the equal-time correlation function of $\langle B^*_i(\boldsymbol{k}, t)B_j(\boldsymbol{k}', t)\rangle = (2\pi)^3\delta^{(3)}(\boldsymbol{k} - \boldsymbol{k}')F_{ij}(\boldsymbol{k}, t)$, where $B_i(\boldsymbol{k}, t)$ is the Fourier transformation of $B_i(\boldsymbol{x}, t)$ [the magnetic component of $A_{\mu\nu}$ in Eq. (3)]. Since parity violation of the Lagrangian is not considered in this

Letter, the antisymmetric part of $F_{ij}(\boldsymbol{k},t)$ vanishes, with $F_{ij}(\boldsymbol{k},t)/(2\pi)^3 = (\delta_{ij} - \hat{k}_i\hat{k}_j)E_M(k,t)/(4\pi k^2)$, and the magnetic energy density is obtained as [21] $\rho_B(t) = \int_0^\infty E_M(k,t)dk$. The MF strength can be obtained as $B_\xi = \sqrt{2d\rho_B/d\log(k)}$. With the "characteristic" correlation length being defined as $\xi_M(t) = \int dk k^{-1} E_M(k,t)/\rho_B(t)$, the corresponding root-mean-square (scale-averaged) MF strength is [62] $B_{\rm rms}(t) = \sqrt{2\rho_B(t)}$.

The GWs sources from the first-order PT mainly include bubble collisions, sound waves, and turbulence. We focus on GWs produced from bubble collisions when the MFs are produced. Recently, significant progress has been made on lattice simulations of the GW production from the first-order PT [27,51–54,57,64,65]. For the calculation approach, we adopt the straightforward procedure detailed in Ref. [66] rather than the envelope approximation, which is still under improvement and cannot tell the whole story (see Refs. [27,57] for recent lattice realization and Refs. [28,29,67,68] for theoretical studies). The EOM of tensor perturbations h_{ij} reads

$$\ddot{h}_{ij} - \nabla^2 h_{ij} = 16\pi G T^{\rm TT}_{ij}. \tag{4}$$

Here the superscript TT denotes the transverse traceless projection, and the energy-momentum tensor is dominated by

$$T_{\mu\nu} = \partial_\mu \Phi^\dagger \partial_\nu \Phi - g_{\mu\nu}\frac{1}{2}{\rm Re}[(\partial_i \Phi^\dagger \partial^i \Phi)], \tag{5}$$

where we neglected the contribution from the subdominant MFs, but the MF's contribution affects the evolution of Higgs field through EOM (see Supplemental Material [55] and Ref. [69]). The energy spectrum of GWs is defined as the GW energy density fraction per logarithmic frequency interval,

$$\Omega_{\rm GW} = \frac{1}{\rho_c}\frac{d\rho_{\rm GW}(k)}{d\ln k}. \tag{6}$$

Numerical results.—Numerical-SimulationOur simulations are performed on a cubic lattice with the resolution 512^3, and the lattice size L^3 is related with the number of bubbles initially placed in the lattice. The time spacing is chosen to be $\Delta t = L/2048$, which is much smaller than the spacial resolution $\Delta x = L/512$. This choice of lattice spacing gives us enough resolution to ensure that we capture all the dynamics for MF and GW production. The mean bubble separation in the simulations is obtained as $R_\star = (L^3/N_b)^{1/3}$, with N_b being the number of the generated bubbles at the simulation, which determines the Lorentz factor for a bubble to be $\gamma_\star = R_\star/(2R_0)$, and the wall width as $L_w^\star = L_w/\gamma_\star$ at bubble collision time. We assume the nucleation rate is a constant during the simulation, which is denoted by p_B [72]. We simulate the cases of $p_B = 10^{-8}$ and $p_B = 10^{-9}$ to investigate the wall thickness effects on the GW and MF productions. For the bubble nucleation rate $p_B = 10^{-8}$, we have $\gamma_\star = 2.98$, with the wall velocity being $v_w = 0.94$ and the mean bubble separation $R_\star \approx 35.6(L_w/\gamma_\star)$ at the time of bubble collision. To reach the thin-wall limit, we consider a much lower nucleation rate $p_B = 10^{-9}$, which yields $\gamma_\star = 4.84$, the wall velocity $v_w = 0.98$, and $R_\star \approx 93.9(L_w/\gamma_\star)$.

The bubble walls are pushed outward by the vacuum energy after bubble nucleation and finally collide with each other. Bubble nucleation scenarios of $p_B = 10^{-8}$ and 10^{-9} are presented to show the connection between the magnetic energy density and the bubble nucleation rate. The two panels of Fig. 1 show that a large p_B predicts an early generation and increase of ρ_B, since the bubbles' nucleation and collision for large p_B occur early (see Fig. 1 in the Supplemental Material [55] for the illustration of bubble expansion and collision.). After the PT, ρ_B constitutes about 1% of the total energy at the end of the simulation, which is much lower than the bounds from the big bang nucleosynthesis, $\rho_B/\rho_{\rm rad} < 0.1$ [73]. To obtain the observables at present, we redshift the GW energy spectrum and MF spectrum by taking into account the temperature T and the duration time of the PT (β^{-1}), which depend on the underlying PT models, and we set them to be free parameters in this Letter.

We first numerically calculate the spectrum of the MF strength generated during the first-order electroweak PT when the GWs are produced (we consider the PT temperature $T = 100$ GeV). As shown in the top panel of Fig. 2, our simulation results in a broken power-law spectrum, with $B_\xi \propto f^{0.91(1.1)}$ for $f < f_\star$ (here $f_\star$ indicates the peak frequency) and $B_\xi \propto f^{-1.65(-0.99)}$ for $f > f_\star$ for $\gamma_\star = 4.84$ with $p_B = 10^{-9}$ ($\gamma_\star = 2.98$ with $p_B = 10^{-8}$), which means that the spectra of MFs from PT can be used to differentiate different bubble collision scenarios. In comparison with a thicker wall ($p_B = 10^{-8}$), the MF spectrum falls off more quickly for a thin-wall scenario ($p_B = 10^{-9}$). (See Fig. 2 in the Supplemental Material [55] for the time evolution of the MF spectra.) The MF strength can reach $B_\xi \sim 10^{-7}$ G at the peak frequency for the thin-wall scenario, with the correlation length being $\xi \sim 10^{-7}$ pc. The effects of the Higgs gradients' contributions [the terms of the second line in Eq. (4)] to the MF generation are also shown there, which emerges after collisions, and increases and dominates the MFs production in the oscillation phase, with the magnitude of MFs increasing by around 3 times after bubble collisions. This characteristic is observed for the first time and strongly supports the MFs production mechanism proposed by Vachaspati and co-workers [20,61]. The MFs spectrum here is different from Ref. [26], where they did not consider the effects of the bubble wall thickness. Taking into account the effects of the hydromagnetic

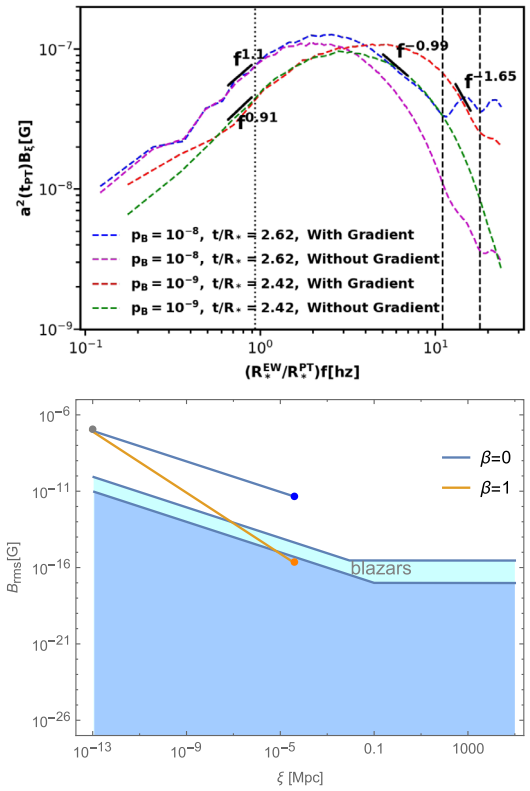

FIG. 2. Top: the frequency-dependent MF spectrum for different times during the first-order PT with $N_b = 160$ (with $\gamma_\star = 2.98$) and $N_b = 36$ (with $\gamma_\star = 4.84$). The length scale associated with the $R_\star$ and L_w are plotted as vertical black dotted line and vertical dashed line. Bottom: the MF strength as a function of correlation length, with cyan and blue regions corresponding to lower bounds set by blazars in Refs. [18,82]. We perform the simulation until the time of $t/R_\star = 2.42, 2.62$ as shown in the top plots, which are long enough for the generation of GWs and MFs, as the stop growth of amplitudes of GW and MF can be found there, see Supplemental Material [55].

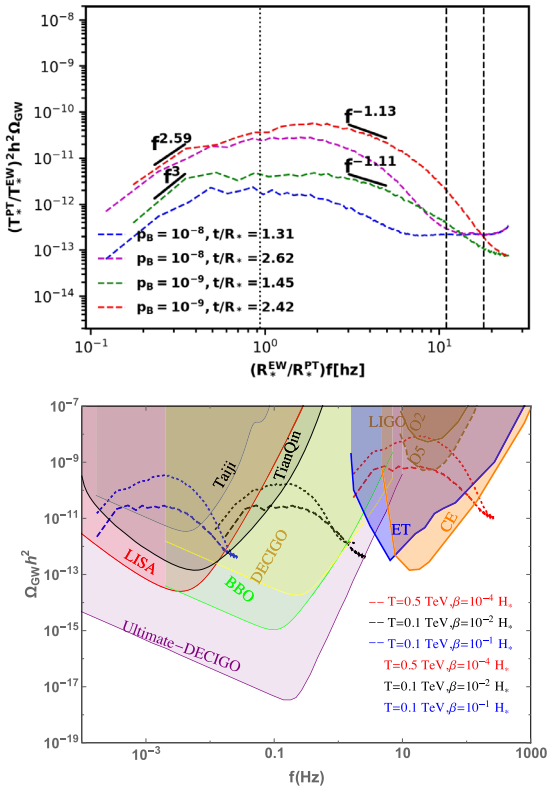

FIG. 3. Top: the frequency-dependent GW energy spectrum for different times during the first-order PT with $N_b = 160$, $\gamma_\star = 2.98$ and $N_b = 36$, $\gamma_\star = 4.84$. The length scale associated with the $R_\star$ and L_w are plotted as the vertical black dotted line and vertical dashed line. Bottom: sensitivity of future GW detectors on the GW spectrum rescaled from the plots in the top panel ($t/R_\star = 1.45$ and $t/R_\star = 2.42$).

turbulence for MFs produced in the electroweak PT allows us to constrain the PT parameter spaces by the cosmic MFs observations. In bottom panel of Fig. 2, we present the bounds on the MFs from the intergalactic MFs blazar observations for the thin-wall scenario. We adopt scaling law that governs the evolution of MFs and the correlation length for the case where MFs do not have enough time to reach the fully helical stage before recombination, as suggested by the numerical simulation of MFs evolution under the magnetohydrodynamic turbulence [62]: $B_{\rm rms} = B_\star(\xi_M/\xi_\star)^{-(\theta+1)/2}$ for $\theta = 0$, 1. We did not present the bounds coming from the big bang nucleosynthesis [74,75] and the spectrum and anisotropies of the cosmic microwave background measurements [76–81], since the two yield null result for the current study.

We now turn to study the property of the GW spectrum generated from the first-order electroweak PT. To show the wall width effects on the GW spectra, we present the GW production from the bubble collisions during the first-order PT with $p_B = 10^{-8}$ and 10^{-9} in the top panel of Fig. 3. In both cases, the GW energy densities increase by around one order from bubble collision to the oscillation phase where MFs are generated (see Fig. 3 in the Supplemental Material [55] for the time evolution of the GW spectra). Our simulation shows that the MF's contribution to the GW production is negligible. We reconfirm the observation of Refs. [27,57,83]: (1) before $t < R_\star$, the dominant contribution to GWs is from the bubble collisions; (2) after $t > R_\star$, the GW energy spectrum continues growing and the peak of $\Omega_{\rm GW}$ shifts toward a higher frequency in the oscillation-coalescence phase. We find that the magnitude of the GW spectrum falls into a valley at the length scale of the wall thickness L_w, and we do not find the negligible contribution of GWs corresponds to the wall thickness observed in Refs. [27,57]. We find that the GW energy spectrum at $t/R_\star = 1.45$ (the bubble collision phase) has a broken power-law form with $\Omega_{\rm GW} \propto f^{3.0,-1.11}$ for infrared and large frequency regions when $p_B = 10^{-9}$, which is consistent with the previous envelope approximation study for the thin-wall limit [67,84–86], where the low-frequency

behavior reveals the causality requirement [87], and the high-frequency behavior is consistent with the analytical calculations [85] in which the single bubble contribution is dominant [88]. At the simulation time of $t/R_* = 2.42$, the GW energy spectrum grows to be $\Omega_{\rm GW} \propto f^{2.59,-1.13}$ in the oscillation phase. Note that $\Omega_{\rm GW} \propto f^3$ in the far infrared region is a universal result as found in Ref. [89]. Since GWs in the infrared region are sourced at the scale larger than R_*, in this case $\Omega_{\rm GW} \propto f^{2.59}$ may result from the limited length scale of the lattice, and also may come from the fact that we fitted this form in the region not very far from the peak frequency; we expect $\Omega_{\rm GW} \propto f^3$ could be reproduced with larger resolution simulations and in the lower frequency region. Similar to the MF production, the behavior of the high-frequency tail of $\Omega_{\rm GW}$ (top panel of Fig. 3) is affected by the oscillations of the Higgs fields in bubble overlap regions during the coalescence stage after the bubble collision. Different PT models can be realized in particular particle physics models beyond the SM, with different PT temperatures (T) and PT duration times (β/H). For example, the electroweak PT can be first-order in the real singlet-extended standard model and standard model effective field theory (see Ref. [37]), with $T = 0.1$ TeV and $\beta = 10^{-2} H_\star$, and the peak frequency of the GW spectrum is located at $f \sim 0.1$ Hz. To illustrate the sensitivities of variant GW detectors (including *LISA* [8], Taiji [9], TianQin [10], DECIGO [12], BBO [11], LIGO [4,90,91], Einstein Telescope [92,93], and Cosmic Explorer [94]) for the GWs produced from variant PT models, we plot the bottom panel of Fig. 3, where the GWs are rescaled from the GW spectra generated with $p_B = 10^{-9}$ at $t/R_\star = 1.45$ (dashed curves) and $t/R_\star = 2.42$ (dotted curves).

Conclusions.—In this Letter, we performed a simultaneous study of the MFs and GWs production at the first-order electroweak PT. Given the evolution of magnetohydrodynamics turbulence after the PT, we obtain the MFs at the characteristic correlation length [62,95] that may seed the observed MFs in galaxy clusters. Our simulation suggests that the MF strength generated from the bubble collisions during the electroweak PT can reach $B_{\rm rms} \sim 10^{-7}$ G at a typical characteristic correlation length $\xi \sim 10^{-7}$ pc. The signature can be used to distinguish the MFs from the PT from other sources of MFs in future observations. We note that, although the maximum MF strength here is comparable with the helical MFs generated by sphaleron decay when *CP* violation shows up [20,96,97], the MF spectrum is totally different, which can be probed by future MF observations. Furthermore, the probe of GW's spectrum at future GW detectors (such as *LISA*) is expected to discriminate GWs from the PT and other GW sources. We therefore establish the possibility for probing the first-order electroweak PT directly through the observation MFs at the correlation length and the detection of its predicted GWs at space-based interferometers. This can serve as an inspection of the underlying new physics beyond the standard model (for practical models' studies of intergalactic MFs and GWs, see Refs. [98,99]).

In the present Letter, we did not consider the interaction between fields and plasma since we focus on the MF and GW generation during the bubble collision stage. For vacuum phase transition where the sound wave is absent, one only needs to consider bubble collisions. Generally, with the interaction between Higgs field and plasma, the predicted GW signal might be amplified to some extent in the high-frequency region in comparison with the case only considering the bubble collision. For that situation, the sound wave will dominate over the GWs from bubble collisions [7]. We expect our observation still holds there and leave the detailed study to another publications. Different GW sources are distinguished by their different spectra. For the GW spectrum produced by the first-order PT, one of the key targets in the space-based GW detectors like *LISA* [8], it is of typical broken power-law shape with different slopes for low and high frequencies [7,100,101].

We thank John T. Giblin, Marek Lewicki, David Weir, Zach Weiner, and Yiyang Zhang for communications. We are grateful to Francesc Ferrer and Tanmay Vachaspati for enlightening discussions. L. B. was supported by the National Natural Science Foundation of China under Grants No. 12075041, No. 11605016, and No. 11947406, Chongqing Natural Science Foundation (Grant No. cstc2020jcyj-msxmX0814), and the Fundamental Research Funds for the Central Universities of China (No. 2019CDXYWL0029). R. G. C. is supported by the National Natural Science Foundation of China Grants No. 11690022, No. 11821505, No. 11991052, and No. 11947302, Strategic Priority Research Program of the Chinese Academy of Sciences Grant No. XDB23030100, and the Key Research Program of Frontier Sciences of CAS.

*lgbycl@cqu.edu.cn
†cairg@itp.ac.cn
‡liujing@ucas.ac.cn

[1] M. D'Onofrio, K. Rummukainen, and A. Tranberg, Phys. Rev. Lett. **113**, 141602 (2014).
[2] D. E. Morrissey and M. J. Ramsey-Musolf, New J. Phys. **14**, 125003 (2012).
[3] N. Arkani-Hamed, T. Han, M. Mangano, and L.-T. Wang, Phys. Rep. **652**, 1 (2016).
[4] B. P. Abbott *et al.* (LIGO Scientific and Virgo Collaborations), Phys. Rev. Lett. **116**, 061102 (2016).
[5] A. Mazumdar and G. White, Rep. Prog. Phys. **82**, 076901 (2019).
[6] C. Caprini *et al.*, J. Cosmol. Astropart. Phys. 04 (2016) 001.
[7] C. Caprini *et al.*, J. Cosmol. Astropart. Phys. 03 (2020) 024.
[8] P. Amaro-Seoane *et al.* (LISA Collaboration), arXiv:1702.00786.

[9] W.-H. Ruan, Z.-K. Guo, R.-G. Cai, and Y.-Z. Zhang, Int. J. Mod. Phys. A **35**, 2050075 (2020).
[10] J. Luo *et al.* (TianQin Collaboration), Classical Quantum Gravity **33**, 035010 (2016).
[11] V. Corbin and N. J. Cornish, Classical Quantum Gravity **23**, 2435 (2006).
[12] K. Yagi and N. Seto, Phys. Rev. D **83**, 044011 (2011); **95**, 109901(E) (2017).
[13] D. G. Yamazaki, T. Kajino, G. J. Mathew, and K. Ichiki, Phys. Rep. **517**, 141 (2012).
[14] J. Xu and J. L. Han, Mon. Not. R. Astron. Soc. **486**, 4275 (2019).
[15] J. L. Han, R. N. Manchester, W. van Straten, and P. Demorest, Astrophys. J. Suppl. Ser. **234**, 11 (2018).
[16] J. Han, Annu. Rev. Astron. Astrophys. **55**, 111 (2017).
[17] C. D. Dermer, M. Cavadini, S. Razzaque, J. D. Finke, J. Chiang, and B. Lott, Astrophys. J. Lett. **733**, L21 (2011).
[18] A. Taylor, I. Vovk, and A. Neronov, Astron. Astrophys. **529**, A144 (2011).
[19] A. Neronov and I. Vovk, Science **328**, 73 (2010).
[20] T. Vachaspati, Phys. Rev. Lett. **87**, 251302 (2001).
[21] R. Durrer and A. Neronov, Astron. Astrophys. Rev. **21**, 62 (2013).
[22] D. Grasso and H. R. Rubinstein, Phys. Rep. **348**, 163 (2001).
[23] K. Subramanian, Rep. Prog. Phys. **79**, 076901 (2016).
[24] A. Kandus, K. E. Kunze, and C. G. Tsagas, Phys. Rep. **505**, 1 (2011).
[25] C. Caprini, R. Durrer, and G. Servant, J. Cosmol. Astropart. Phys. 12 (2009) 024.
[26] Y. Zhang, T. Vachaspati, and F. Ferrer, Phys. Rev. D **100**, 083006 (2019).
[27] D. Cutting, E. G. Escartin, M. Hindmarsh, and D. J. Weir, Phys. Rev. D **103**, 023531 (2021).
[28] M. Lewicki and V. Vaskonen, Eur. Phys. J. C **80**, 1003 (2020).
[29] M. Lewicki and V. Vaskonen, Eur. Phys. J. C **81**, 437 (2021).
[30] A. Diaz-Gil, J. Garcia-Bellido, M. Garcia Perez, and A. Gonzalez-Arroyo, Phys. Rev. Lett. **100**, 241301 (2008).
[31] A. Diaz-Gil, J. Garcia-Bellido, M. Garcia Perez, and A. Gonzalez-Arroyo, J. High Energy Phys. 07 (2008) 043.
[32] C. Grojean, G. Servant, and J. D. Wells, Phys. Rev. D **71**, 036001 (2005).
[33] C. Grojean and G. Servant, Phys. Rev. D **75**, 043507 (2007).
[34] R.-G. Cai, M. Sasaki, and S.-J. Wang, J. Cosmol. Astropart. Phys. 08 (2017) 004.
[35] S. Profumo, M. J. Ramsey-Musolf, C. L. Wainwright, and P. Winslow, Phys. Rev. D **91**, 035018 (2015).
[36] R. Zhou, L. Bian, and H.-K. Guo, Phys. Rev. D **101**, 091903(R) (2020).
[37] R. Zhou, L. Bian, H.-K. Guo, and Y. Wu, Phys. Rev. D **101**, 035011 (2020).
[38] A. Alves, T. Ghosh, H.-K. Guo, K. Sinha, and D. Vagie, J. High Energy Phys. 04 (2019) 052.
[39] S. Profumo, M. J. Ramsey-Musolf, and G. Shaughnessy, J. High Energy Phys. 08 (2007) 010.
[40] J. R. Espinosa, T. Konstandin, and F. Riva, Nucl. Phys. **B854**, 592 (2012).
[41] M. Jiang, L. Bian, W. Huang, and J. Shu, Phys. Rev. D **93**, 065032 (2016).
[42] J. M. Cline, K. Kainulainen, and M. Trott, J. High Energy Phys. 11 (2011) 089.
[43] G. Dorsch, S. Huber, and J. No, J. High Energy Phys. 10 (2013) 029.
[44] G. C. Dorsch, S. J. Huber, K. Mimasu, and J. M. No, Phys. Rev. Lett. **113**, 211802 (2014).
[45] J. Bernon, L. Bian, and Y. Jiang, J. High Energy Phys. 05 (2018) 151.
[46] J. O. Andersen, T. Gorda, A. Helset, L. Niemi, T. V. I. Tenkanen, A. Tranberg, A. Vuorinen, and D. J. Weir, Phys. Rev. Lett. **121**, 191802 (2018).
[47] K. Kainulainen, V. Keus, L. Niemi, K. Rummukainen, T. V. Tenkanen, and V. Vaskonen, J. High Energy Phys. 06 (2019) 075.
[48] R. Zhou, W. Cheng, X. Deng, L. Bian, and Y. Wu, J. High Energy Phys. 01 (2019) 216.
[49] L. Bian, H.-K. Guo, and J. Shu, Chin. Phys. C **42**, 093106 (2018); **43**, 129101(E) (2019).
[50] S. J. Huber, T. Konstandin, G. Nardini, and I. Rues, J. Cosmol. Astropart. Phys. 03 (2016) 036.
[51] M. Hindmarsh, S. J. Huber, K. Rummukainen, and D. J. Weir, Phys. Rev. Lett. **112**, 041301 (2014).
[52] D. Cutting, M. Hindmarsh, and D. J. Weir, Phys. Rev. Lett. **125**, 021302 (2020).
[53] M. Hindmarsh, S. J. Huber, K. Rummukainen, and D. J. Weir, Phys. Rev. D **92**, 123009 (2015).
[54] M. Hindmarsh, S. J. Huber, K. Rummukainen, and D. J. Weir, Phys. Rev. D **96**, 103520 (2017); **101**, 089902(E) (2020).
[55] See Supplemental Material at http://link.aps.org/supplemental/10.1103/PhysRevLett.126.251102 for the bubble nucleation and collision process, and the generations of MFs and GWs, which includes Refs. [27,51,56,57].
[56] M. Hindmarsh and M. Hijazi, J. Cosmol. Astropart. Phys. 12 (2019) 062.
[57] D. Cutting, M. Hindmarsh, and D. J. Weir, Phys. Rev. D **97**, 123513 (2018).
[58] A. Rajantie, P. M. Saffin, and E. J. Copeland, Phys. Rev. D **63**, 123512 (2001).
[59] Y. Zhang, F. Ferrer, and T. Vachaspati, Phys. Rev. D **96**, 043014 (2017).
[60] G. 't Hooft, Nucl. Phys. **B79**, 276 (1974).
[61] T. Vachaspati, Phys. Lett. B **265**, 258 (1991).
[62] A. Brandenburg, T. Kahniashvili, S. Mandal, A. R. Pol, A. G. Tevzadze, and T. Vachaspati, Phys. Rev. D **96**, 123528 (2017).
[63] A. Brandenburg, R. Durrer, T. Kahniashvili, S. Mandal, and W. W. Yin, J. Cosmol. Astropart. Phys. 08 (2018) 034.
[64] J. T. Giblin and J. B. Mertens, Phys. Rev. D **90**, 023532 (2014).
[65] A. R. Pol, S. Mandal, A. Brandenburg, T. Kahniashvili, and A. Kosowsky, Phys. Rev. D **102**, 083512 (2020).
[66] J. Garcia-Bellido, D. G. Figueroa, and A. Sastre, Phys. Rev. D **77**, 043517 (2008).
[67] T. Konstandin, J. Cosmol. Astropart. Phys. 03 (2018) 047.
[68] J. Ellis, M. Lewicki, and V. Vaskonen, J. Cosmol. Astropart. Phys. 11 (2020) 020.

[69] The GWs generated from MFs is negligible since the energy density of MFs is subdominant. The peak of the energy spectrum of GWs from MFs is estimated as 10^{-13} using the method of Ref. [70], which is much smaller than that from bubble collision, 10^{-9}. Reference [71] presented the possibility to constrain the small scale MFs with the GW detection with the pulsar timing array experiments.
[70] C. Caprini and R. Durrer, Phys. Rev. D **74**, 063521 (2006).
[71] S. Saga, H. Tashiro, and S. Yokoyama, Phys. Rev. D **98**, 083518 (2018).
[72] I. G. Garcia, S. Krippendorf, and J. March-Russell, Phys. Lett. B **779**, 348 (2018).
[73] V. Mukhanov, *Physical Foundations of Cosmology* (Cambridge University Press, Oxford, 2005), ISBN 978-0-521-56398-7.
[74] T. Kahniashvili, A. G. Tevzadze, S. K. Sethi, K. Pandey, and B. Ratra, Phys. Rev. D **82**, 083005 (2010).
[75] M. Kawasaki and M. Kusakabe, Phys. Rev. D **86**, 063003 (2012).
[76] T. R. Seshadri and K. Subramanian, Phys. Rev. Lett. **103**, 081303 (2009).
[77] P. A. R. Ade *et al.* (Planck Collaboration), Astron. Astrophys. **594**, A19 (2016).
[78] K. Jedamzik, V. Katalinic, and A. V. Olinto, Phys. Rev. Lett. **85**, 700 (2000).
[79] J. D. Barrow, P. G. Ferreira, and J. Silk, Phys. Rev. Lett. **78**, 3610 (1997).
[80] R. Durrer, P. G. Ferreira, and T. Kahniashvili, Phys. Rev. D **61**, 043001 (2000).
[81] P. Trivedi, K. Subramanian, and T. R. Seshadri, Phys. Rev. D **82**, 123006 (2010).
[82] M. Ackermann *et al.* (Fermi-LAT Collaboration), Astrophys. J. Suppl. Ser. **237**, 32 (2018).
[83] H. L. Child and J. T. Giblin Jr., J. Cosmol. Astropart. Phys. 10 (2012) 001.
[84] A. Kosowsky and M. S. Turner, Phys. Rev. D **47**, 4372 (1993).
[85] S. J. Huber and T. Konstandin, J. Cosmol. Astropart. Phys. 09 (2008) 022.
[86] C. Caprini, R. Durrer, T. Konstandin, and G. Servant, Phys. Rev. D **79**, 083519 (2009).
[87] M. Maggiore, *Gravitational Waves. Vol. 2: Astrophysics and Cosmology* (Oxford University Press, New York, 2018), ISBN 978-0-19-857089-9.
[88] R. Jinno and M. Takimoto, Phys. Rev. D **95**, 024009 (2017).
[89] R.-G. Cai, S. Pi, and M. Sasaki, Phys. Rev. D **102**, 083528 (2020).
[90] E. Thrane and J. D. Romano, Phys. Rev. D **88**, 124032 (2013).
[91] B. Abbott *et al.* (LIGO Scientific and Virgo Collaborations), Phys. Rev. D **100**, 061101 (2019).
[92] S. Hild *et al.*, Classical Quantum Gravity **28**, 094013 (2011).
[93] M. Punturo *et al.*, Classical Quantum Gravity **27**, 194002 (2010).
[94] B. P. Abbott *et al.* (LIGO Scientific Collaboration), Classical Quantum Gravity **34**, 044001 (2017).
[95] T. Kahniashvili, A. G. Tevzadze, A. Brandenburg, and A. Neronov, Phys. Rev. D **87**, 083007 (2013).
[96] C. J. Copi, F. Ferrer, T. Vachaspati, and A. Achucarro, Phys. Rev. Lett. **101**, 171302 (2008).
[97] J. M. Cornwall, Phys. Rev. D **56**, 6146 (1997).
[98] J. Ellis, M. Fairbairn, M. Lewicki, V. Vaskonen, and A. Wickens, J. Cosmol. Astropart. Phys. 09 (2019) 019.
[99] J. Ellis, M. Fairbairn, M. Lewicki, V. Vaskonen, and A. Wickens, J. Cosmol. Astropart. Phys. 10 (2020) 032.
[100] C. Caprini, D. G. Figueroa, R. Flauger, G. Nardini, M. Peloso, M. Pieroni, A. Ricciardone, and G. Tasinato, J. Cosmol. Astropart. Phys. 11 (2019) 017.
[101] C. Caprini and D. G. Figueroa, Classical Quantum Gravity **35**, 163001 (2018).